Nuclear Physics A 4561 (1999) 1–99

Measurements of proton radiative capture cross sections relevant to the astrophysical rp- and γ-processes

F.R. Chloupek [a], A. St J. Murphy [a], R.N. Boyd [a,b], A.L. Cole [a], J. Görres [c], R.T. Guray [a], G. Raimann [a], J.J. Zach [a], T. Rauscher [d], J.V. Schwarzenberg [c], P. Tischhauser [c], M.C. Wiescher [c]

[a] *Department of Physics, The Ohio State University, Columbus, OH, 43210, USA*
[b] *Department of Astronomy, The Ohio State University, Columbus, OH 43210, USA*
[c] *Department of Physics, University of Notre Dame, South Bend, IN 46656, USA*
[d] *Departmentfür Physik und Astronomie, Universität Basel, Klingelbergstr, 82, CH-4056 Basel, Switzerland*

Received 2 February 1999; revised 12 April 1999; accepted 22 April 1999

Abstract

Measurements have been made of the ^{96}Zr(p,γ)^{97}Nb, ^{112}Sn(p,γ)^{113}Sb, and ^{119}Sn(p,γ)^{120}Sb cross section excitation functions. Incident proton energies ranged from 2.8 MeV to 8.5 MeV. These reactions are relevant to several processes of stellar nucleosynthesis. The resulting astrophysical S-factors are compared to those from theoretical statistical model calculations using the SMOKER, and the more recent NON-SMOKER, codes to judge their applicability to these reactions.

Keywords: Astrophysical S-factors; p-process; Nuclear cross sections; Proton radiative capture reactions

1. Introduction

The p-process nuclei are the proton-rich nuclides that are blocked from production in the r- or s-processes by stable nuclei. The "p-process" actually is thought to consist of several different sub-processes, including the γ-process [1], which operates through a series of photodissociation reactions on abundant heavy seed nuclides; the rp-process [2–4], which is driven by a series of rapid proton captures on abundant light seed nuclei; the α-process [5,6], in which nuclei are synthesized via a variety of reactions that occur in nuclear statistical equilibrium; and the ν-process [7], which occurs during the

PII S0375-9474(99)00167-0

neutrino wind that accompanies the final stage of core collapse of a massive star. The various mechanisms by which the p-process nuclides may be synthesized have been reviewed in several recent papers [8–10] .

Calculation of the abundances of the p-process nuclides typically requires extensive numbers of reaction rates, many of which are often for either (p,γ) or (γ,p) reactions. Very few cross sections relevant to these processes, which involve light ions on relatively heavy nuclei, have been measured at energies appropriate to astrophysics, leaving these reaction networks dependent upon theoretical estimates calculated through statistical models [11–17] . The cross sections on heavy nuclides that are relevant to these models that have been experimentally determined include (p,γ) reactions on ^{92}Mo, ^{94}Mo, ^{95}Mo, ^{98}Mo [18] , ^{96}Ru, ^{98}Ru, ^{99}Ru, ^{104}Ru [19] , ^{90}Zr [20] , and ^{142}Ce [21] targets; and (α,γ) reactions on ^{70}Ge [22] , ^{139}La [21] , and ^{144}Sm [23] targets.

This work presents experimental results for three previously unmeasured (p,γ) cross section excitation functions in an attempt to expand the experimental knowledge base of these reactions. Those results are then compared to the calculated results of the statistical model codes NON-SMOKER [17,24] , and its predecessor, SMOKER [14,15] .

An activation technique was used in this study, which allowed for the measurement of (p,γ) cross section excitation functions at the energies required for target nuclei in the medium to heavy mass range. However, this limited the reactions that could be studied to those where the product nuclei are radioactive, and have half-lives in a range appropriate to this technique. As such, the focus of this experiment is on testing the applicability of statistical model calculations, rather than measuring specific key p-process reactions.

Section 2 describes the experimental technique and apparatus used to make the measurements. Section 3 presents the experimental results and compares them to astrophysical *S*-factors calculated by the statistical model codes SMOKER and NON-SMOKER. Conclusions from this study are given in Section 4.

2. Experimental procedure

The data were collected at the FN Tandem Van de Graaff accelerator facility at the University of Notre Dame. The ^{112}Sn(p,γ)^{113}Sb reaction ($Q = 3.05$ MeV) was measured over a range of incident proton energies from 3.0 to 8.5 MeV, the ^{119}Sn(p,γ)^{120}Sb reaction ($Q = 5.64$ MeV) from 2.8 to 6.5 MeV, and the ^{96}Zr(p,γ)^{97}Nb reaction ($Q = 7.46$ MeV) from 3.5 to 6.0 MeV. The low ends of these energy ranges overlap, or are close to, the Gamow windows predicted for these reactions in the high temperature environments in which they are of interest. Explicitly, the Gamow windows at a temperature of 2×10^9 Kelvin for the three reactions are 2.26 ± 0.72 MeV (FWHM) for the ^{96}Zr(p,γ)^{97}Nb reaction, and 2.62 ± 0.78 MeV for the two reactions on the tin isotopes. The incident proton energies were varied in approximately 250 keV steps for the lower energies and 500 keV for the upper energies, with a typical beam current on target of 100–150 nA.

The length of irradiation was chosen based upon the half-life of the (p,γ) activation

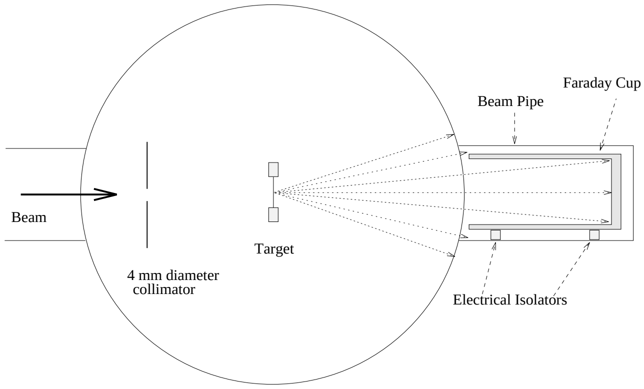

Fig. 1. Diagram of the scattering chamber, illustrating how angular straggling of the beam after passing through the target caused falsely low beam currents to be measured with the target in place. The true beam current was determined from target out runs.

product. In the cases of the ^{112}Sn and ^{119}Sn targets, where the (p,γ) reaction products are ^{113}Sb ($t_{1/2}$ = 6.67 m) and ^{120}Sb ($t_{1/2}$ = 15.9 m), the irradiations lasted approximately 4 half-lives. In the case of the ^{96}Sn(p,γ)^{97}Nb reaction, where the reaction product has a half-life of 72 m, the target was irradiated for about 2 half-lives. This ensured that a large fraction of the maximum possible activation was achieved without the possibility of target degradation.

The combination of low beam energy and relatively thick self-supporting foil targets resulted in a significant fraction of the beam scattering from the target and striking the beam pipe upstream from the Faraday cup (see Fig. 1). The amount of scatter depended on the energy of the proton beam, ranging from 20% up to 65% for the lowest incident proton energies, an amount consistent with angular straggling predicted by the program `STOPX` [25]. The integrated beam current incident upon the Faraday Cup was measured at regular intervals to determine its degree of variation during the irradiation. Its value was stable to within 3% over the duration of each irradiation. Because of the aforementioned scattering, it was necessary to measure the true incident beam current with the target removed.

Several other measures were taken to ensure that the beam current measurements were accurate. Firstly, the beam was collimated with a 4 mm diameter hole held in front of the target, and focused prior to the irradiations through a similar aperture at the target position. Current measurements taken from these confirmed an excellent beam quality. Secondly, to ensure complete electron suppression two measures were taken: the Faraday Cup was held at a bias of −300 V, and two Neodymium magnets (PASCO EM-8621), each having a residual flux density of 10500–11000 Gauss, were placed close to the target.

After each irradiation, the target was taken to a separate low background counting area. The ^{112}Sn and ^{119}Sn targets were placed between two bismuth germanate (BGO) detectors surrounded by stainless steel (a 1.9 cm thick cylinder) and lead shielding (over 10 cm thick), and covered by active plastic scintillator cosmic ray veto counters. This

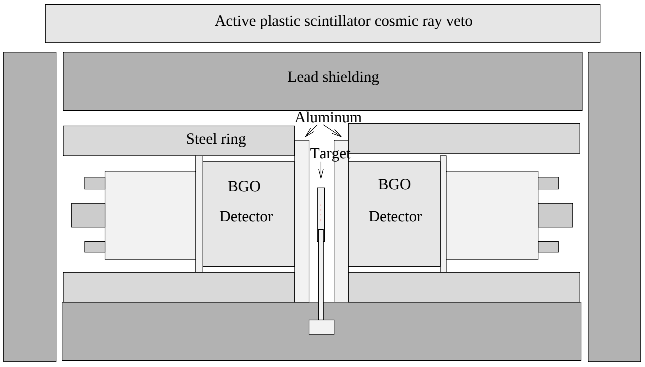

Fig. 2. Diagram of the BGO detector set-up (not to scale).

Table 1
Properties of the targets used in this work

Target	Thickness (mg/cm^2)	purity	major contaminants (%)
^{12}C	100	—	—
^{96}Zr	3.98	57.36	^{90}Zr (9.19), ^{91}Zr (2.02) ^{92}Zr (27.20), ^{94}Zr (4.22)
^{112}Sn	2.7	98.90	^{114}Sn (1.00)
^{119}Sn	2.6	89.80	^{116}Sn (0.65), ^{117}Sn (0.63), ^{118}Sn (3.01) ^{120}Sn (5.34), ^{122}Sn (0.28), ^{124}Sn (0.27)

setup is shown in Fig. 2. Decays were observed for at least four product half-lives for the tin isotopic targets. A high-purity germanium (HPGe) detector was also used to observe the γ-ray spectra of the irradiated ^{112}Sn and ^{119}Sn targets at high resolution to obtain accurate energy calibrations of the emissions of the ^{113}Sb and ^{120}Sb products, as well as to determine if there were any additional radioactive elements in the irradiated target. For most of the runs with the tin targets, though, the BGO detectors were preferable because of their much higher efficiency. The ^{96}Zr target was placed next to a HPGe detector inside the lead shielding to observe the ^{97}Nb decays, which were observed for over one product half-life. The high resolution of the HPGe detector was necessary to resolve the numerous γ-ray peaks from ^{96}Nb produced by the ^{96}Zr(p,n)^{96}Nb reaction.

Two of the targets used in the experiment, ^{112}Sn and ^{119}Sn, were borrowed from the Indiana University Cyclotron Facility. The relevant properties of all the targets used are listed in Table 1. The enrichments were determined with spark-source mass spectroscopic analysis. The foils were rolled many times with a light rolling pressure, and turned 90 degrees after each pass, then trimmed and the areas were calculated from the dimensions. Each was then weighed with an analytical balance ($\pm 50\ \mu$g) before being mounted to make self-supporting targets.

In addition, a relatively thick ^{12}C target was irradiated at the highest energy used in our measurements. This was then viewed with the HPGe detectors to determine whether carbon build up on the targets could contribute a significant yield to our measurements.

The irradiated carbon target did not show significant activation compared to that observed with our Zr and Sn targets at even our lowest energies, showing that carbon build up was not a concern in these measurements.

The products of the ^{112}Sn(p,γ) and ^{119}Sn(p,γ) reactions, ^{113}Sb and ^{120}Sb, both decay by positron emission. Thus, the 511 keV γ-rays produced by the eventual annihilation of the positrons were used to detect these decays. Aluminum plates were placed between the detector and the target to stop the positrons.

To calculate the detector efficiency for a specific γ-ray energy, a Monte Carlo simulation of the experiment was developed by the authors. The target was treated as a point source located a distance from the detectors corresponding to the set-up shown in Fig. 2. Then the absolute efficiency for each relevant γ-ray was calculated by simulating the emission of γ-rays at that energy with an isotropic random distribution of angles, while taking into account absorption/scattering in the aluminum and the fraction of the photons that are absorbed in the BGO photopeak. Where possible the Monte Carlo was calibrated with, and tested against, standard gamma-ray calibration sources.

The "source" for the 511 keV γ-rays, however, was diffuse because of the motion of the positrons. Therefore, to calculate the BGO efficiency for the 511 keV γ-rays, the simulation assumed an isotropic emission of positrons at random angles, with energies distributed according to the expected positron spectrum. The positrons were assumed to stop once they had penetrated an appropriate distance into the aluminum absorber [26] , lead shielding, or target frame. Their subsequent annihilations with electrons created two 511 keV γ-rays emerging back to back at another randomly chosen angle. The probability of each photon being detected was calculated, resulting in the efficiency for 511 keV γ-ray singles. The Monte Carlo program tracked both γ-rays, thus also allowing for the computation of the efficiency for 511 keV γ-ray coincidences in both detectors.

For each BGO event four parameters were recorded; the time difference between the two detector signals as measured by a time-to-amplitude converter (TAC), the energy signals from both detectors, and a scaler reading of a clock value based on a high precision 1 kHz quartz oscillator. This clock signal was also gated on the data acquisition busy signal and sent to a separate scaler to provide accurate live time information. For each HPGe event two parameters were recorded: an energy signal and a clock value. The live time of the experiment was again determined through the use of a high precision 1 kHz quartz oscillator. The efficiency of the HPGe detector was determined using a ^{137}Cs source since the energy of its single decay line is almost identical to the one we wished to measure.

3. Analysis and results

3.1. Spectra

Each activated target was initially viewed by a HPGe detector to identify the γ-ray peaks with high resolution. In the spectrum from the irradiated ^{112}Sn target a number of γ-ray peaks from ^{113}Sb decay were identified. A peak at 1009 keV was determined to result from a summed 511 keV γ-ray resulting from a positron annihilation and subsequent 498 keV γ-ray from the decay of an excited state of the daughter nucleus ^{113}Sn. There was an additional peak from the decay of ^{113}Sn to ^{113}In ($t_{1/2}=115$ days), which produces a 392 keV γ-ray.

A similar procedure was used to determine the γ-ray spectra of the irradiated ^{119}Sn and ^{96}Zr targets. The spectra from the ^{119}Sn target contained γ-rays not only from ^{120}Sb, but also small contributions from products of reactions involving other tin isotopes present in the target. The irradiated ^{96}Zr spectrum was more complex, partly due to contamination from other zirconium isotopes in the target, but mostly from the (p,n) reaction on ^{96}Zr, producing ^{96}Nb ($t_{1/2}=23.4$ hours). The decays of ^{97}Nb could only be observed using the HPGe detector, since the 658 keV γ-ray from ^{97}Nb could not otherwise be separated from the other decay products (both β-rays and γ-rays) of ^{96}Nb and other contaminants with the BGOs.

Potential contributions to the overall background in these experiments included the room background, carbon buildup, and isotopic impurities. The room background was minimized by the use of active and passive shielding, and as mentioned earlier, an irradiation of a ^{12}C target determined that carbon buildup was not significant in any of the measurements.

Given the dominance of the Compton scattered photons, the remaining room background was combined with the Compton scattering as part of an overall background function. The shape and relative height of this function was determined by use of the Monte Carlo code, with the photopeak contributions (photoelectric effect) removed. This showed that in most cases a simple exponential would represent well the non-photopeak contributions to the spectra. The one case where this was not satisfactory was for the ^{119}Sn(p,γ) data, where the dominance of a single, well-separated peak meant that an exponential shape was not adequate. The shape suggested by the Monte Carlo was well represented by a 5th order polynomial. The immediate improvement in the quality of the curve fitting, together with the excellent representation of the spectra by the Monte Carlo for all other data sets, gives us confidence in this approach.

The singles spectra from the irradiated ^{112}Sn target were fit with Gaussians for the 498–511 keV peak, the 935–1018 keV peak, and the 334 keV peak (with the area constrained to that of the 498–511 keV peak). Additionally, a correction was made for the 392 keV γ-ray from ^{113}Sn. A typical spectrum, along with the individual peak fits and overall composite fit, is shown in Fig. 3.

The coincidence spectra from the irradiated ^{112}Sn target were obtained by requiring a TAC signal and an event in the 498–511 peak in the other BGO detector. These spectra were fitted with a procedure similar to the singles spectra except that, because of the coincidence requirement, the small area of the peak for the 935–1018 keV γ-rays was constrained to the magnitude of the 498–511 keV peak using the known branching ratios. A typical spectrum, along with the peak fits and overall fit, is shown in Fig. 4.

The fitting of the spectra from the irradiated ^{119}Sn target proceeded similarly to those from the ^{112}Sn target except that only the 511 keV peak was significant. The spectra

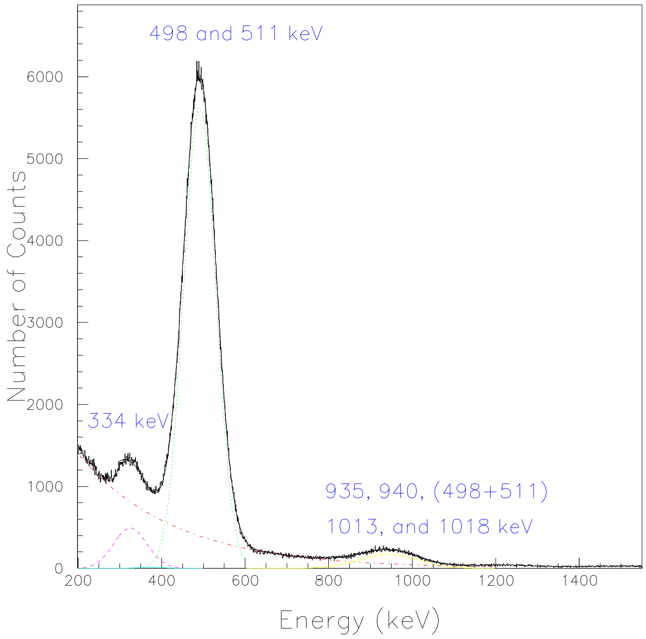

Fig. 3. Sample γ-ray singles spectrum from one of the BGO detectors for the ^{112}Sn target irradiated at an incident proton energy of 7.00 MeV. The components of the fit and the total fit are also plotted.

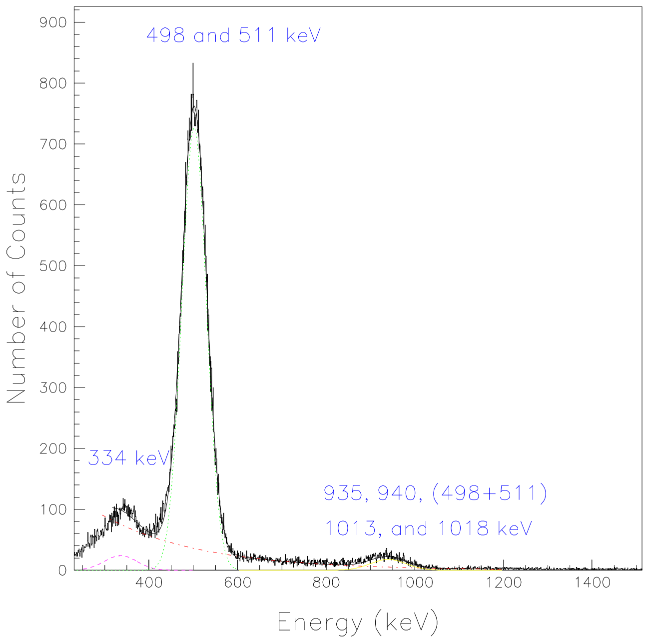

Fig. 4. Sample γ-ray coincident spectrum from one of the BGO detectors for the ^{112}Sn target irradiated at an incident proton energy of 7.00 MeV. The components of the fit and the total fit are also plotted.

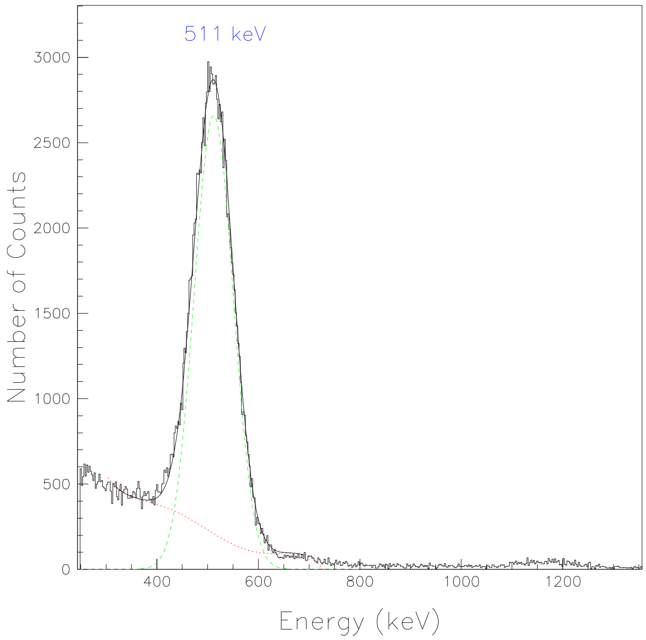

Fig. 5. Sample γ-ray singles spectrum from one of the BGO detectors for the ^{119}Sn target irradiated at an incident proton energy of 4.50 MeV. The components of the fit and the total fit are also plotted.

were fitted with a Gaussian plus a polynomial for the background. The form of this polynomial, together with its scaling relative to the photopeak, was determined from the Monte Carlo as described earlier.

The HPGe detector was used to detect the decay products from the irradiated ^{96}Zr target. An expanded view of a typical spectrum is shown in Fig. 6. The γ-ray peak sits atop a background produced by various β-decays of target products and Compton tails.

3.2. Determination of the cross sections

The decay observations were divided into time intervals, resulting in a number of different spectra, hence cross section measurements, at each energy. In addition, three different measurements of the cross section from each detector at each energy were deduced for the ^{112}Sn(p,γ)^{113}Sb reaction: one from the 498–511 keV peak, one from the 935–1018 keV peak, and one from the 511 keV coincidence peak. For the ^{119}Sn(p,γ)^{120}Sb reaction two separate measurements of the cross section from each detector were obtained for each energy: one from the 511 keV singles peak and the other from the 511 keV coincidence peak. Although these different determinations are not totally independent, it was nonetheless encouraging that there was good agreement between them. A weighted mean of the different measurements was used to arrive at the final value.

In the case of the ^{96}Zr(p,γ)^{97}Nb reaction, the individual cross sections from the different time intervals were averaged to get an overall value at each energy. The long

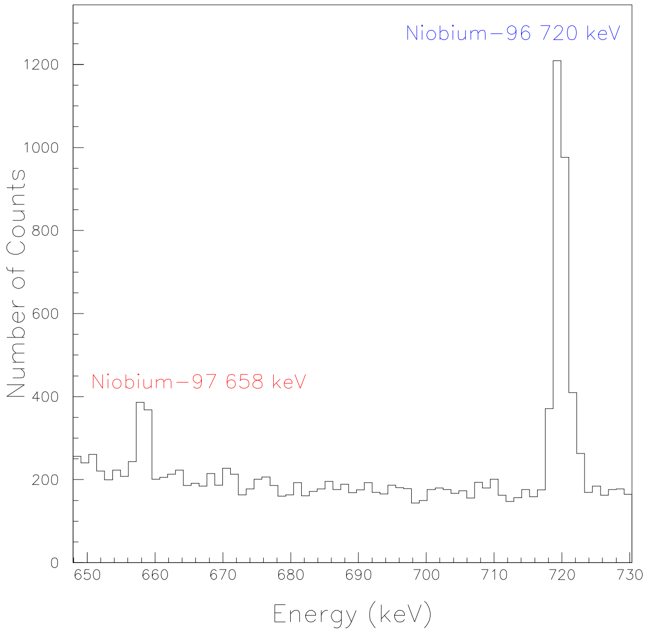

Fig. 6. Sample γ-ray singles spectrum of the HPGe detector for the ^{96}Zr target irradiated at an incident proton energy of 3.75 MeV.

lifetime of ^{97}Nb meant that data were taken for fewer half-lives than for the tin targets, which in turn meant that there were significant counts in the 658 keV peak even in the later intervals. This also necessitated a significant correction for the nuclei left over from earlier irradiations, even though this was minimized by beginning the irradiations with the lowest proton energies and progressively moving to higher energies.

For all targets, the number of nuclides that exist at the end of each irradiation period that were created during that period, denoted by N_{irr}, is given by

$$N_{\rm irr} = I N_t \sigma \left[1 - \exp(-t_{\rm irr}/\tau) \right] \tau, \tag{1}$$

where I is the number of protons per second in the incident beam, N_t is the target density in nuclei cm^{-2}, σ is the (p,γ) cross section, τ is the lifetime of the daughter nuclide of interest, and $t_{\rm irr}$ is the time of the irradiation. Denoting the time between the end of the irradiation period to the beginning of each subsequent counting period as t_1, and the number of daughter nuclei that were left over from previous irradiations and counting periods at the end of the most recent irradiation period as $N_{\rm left}$, then the number of decays that will occur in counting interval $t_2 - t_1$, $N_{\rm decay}$, will be

$$N_{\rm decay} = (N_{\rm irr} + N_{\rm left}) \exp(-t_1/\tau) \left(1 - \exp[-(t_2 - t_1)/\tau]\right). \tag{2}$$

Combining this equation with the detector efficiency and acquisition system live time then gives the rate at which decay events were observed.

Some additional corrections had to be included, however, for the ^{112}Sn(p,γ)^{113}Sb study in particular. The dominant peak in that spectrum resulted from either a 498 keV or a 511 keV γ-ray. However, those γ-rays are sometimes produced in the same decay event. If both γ-rays end up in the same detector, they can result in a higher energy event, and therefore, removal of these events from the dominant peak. Thus, the effective magnitude of the primary peak had to be increased from that observed to account for this effect. This correction was about 8%; it was the largest of the corrections of this type that had to be made. Known branching ratios were used to relate the observed peaks to the cross sections that produced them.

Another type of correction had to be made for the ^{119}Sn(p,γ)^{120}Sb reaction data. Significant impurities of ^{116}Sn and ^{120}Sn exist in that target. The former can produce ^{117}Sb, the decays of which would not be distinguishable from those of ^{120}Sb. The latter can interact through the ^{120}Sn(p,n)^{120}Sb, producing the same daughter nuclide that we were trying to study. This contribution to the total amount of ^{120}Sb produced was calculated by using the cross section measurements of Johnson et al. [27], and interpolating when needed. This resulted in a correction of up to 15% at the highest energies.

The amounts of nuclei created by possible contamination reactions were estimated, using the Johnson et al. [27] data if available, and the NON-SMOKER code output of Rauscher, Thielemann, and Kratz [16,24] for experimentally undetermined reactions. These reactions were generally found not to contribute significantly to the radiation yield. Of those reactions that had not been experimentally studied ^{116}Sn(p,γ)^{117}Sb was identified as the most likely contributor of positrons at a significant level if the NON-SMOKER calculation appreciably underestimated the actual cross section strength. However, that reaction was recently experimentally studied [28]. It was found to contribute a less than 2% contaminant to the overall 511 keV γ-ray yield in the present measurements of the ^{119}Sn(p,γ)^{120}Sb reaction.

The energies indicated in the graphs are mean center of mass energies. Note that, since the reactions are distributed over a range of energies spanning 100–150 keV, the measurements will not be sensitive to resonances significantly narrower than this.

3.3. Uncertainties

The statistical uncertainties in the peak areas ranged from less than 1% to over 10%. The live time measurements and the uncertainties due to the current measurement also constituted a source of error. An additional uncertainty was associated with the geometric placement of the target with respect to the detectors. To calculate this contribution, one sigma uncertainties in each of the relevant geometric placement parameters were estimated and then the Monte Carlo was used to compute the corresponding overall uncertainties. Potentially, the most significant source of uncertainty results from a misalignment in the target placement along the axis between the detectors. However, this is cancelled to first order (to better than 1%) by using a symmetric arrangement with two detectors and averaging their yields.

Possible systematic uncertainties resulted from the geometric set up of the experiment which the Monte Carlo was used to estimate, the branching ratios for the decays, the calculation of the absorption of γ-rays in the aluminum and steel, and uncertainties in the γ-ray detection efficiency. The major contributions were from a possible small offset in the distance between the target and detector (5%), the BGO efficiency calibration (3%), and the target height offset (3%). The uncertainties were added in quadrature to obtain an overall value of the systematic uncertainty.

For those measurements made with the HPGe detector, a 5% overall uncertainty was associated with the target placement. This was added in quadrature with the uncertainties in the HPGe efficiency calibration, current measurements, and live times to get an overall uncertainty.

3.4. Final results

The primary quantity of interest to astrophysics is the astrophysical *S*-factor, defined as

$$S(E) = E\sigma(E)e^{2\pi\eta}, \qquad (3)$$

where $\eta = Z_1 Z_2 e^2/\hbar v$ is the Sommerfeld parameter, with Z_1 and Z_2 as the proton numbers of the interacting particles and v their relative velocity. Plots of the *S*-factors obtained in the present study are shown in Figs. 7, 8, and 9. The data are shown in the figures as individual points with error bars. The curves are the results of the theoretical calculations using the NON-SMOKER code, utilizing a microscopic proton potential [29] and a novel level density description [16]. Also shown are the results of the SMOKER code [14,15]. For completeness, the experimental results are also tabulated in Tables 2, 3 and 4.

Generally the model predictions of the data are reasonable, especially for the ^{96}Zr(p,γ) reaction. The NON-SMOKER predictions in the ^{112}Sn(p,γ) case are somewhat high, and are generally a bit low for ^{119}Sn(p,γ). The differences, however, are at the 25–50% level, not a surprising range of variation given the possible deformations present in these nuclei. It is also noteworthy that the NON-SMOKER prediction is somewhat skewed with respect to the data for the ^{112}Sn(p,γ) case. Notice also that the experimental and theoretical *S*-factors in Fig. 7 decline due to the opening of the (p,n) channel at 7.8 MeV.

4. Conclusions

The present data extend the experimental knowledge of (p,γ) reactions into the mass ranges around $A \approx 100$–120. As the experimental results are fairly consistent with the NON-SMOKER calculations, one would not anticipate a refinement of this code based upon these data to have a great effect. Neither would one expect dramatic changes in the abundance predictions of the p-process codes dependent upon these reactions. Even the reaction closest to the proton drip line, ^{112}Sn(p,γ)^{113}Sb, is in reasonable agreement

Table 2
Tabulation of the ^{112}Sn(p,γ)^{113}Sb reaction experimental results from this study. Uncertainties include both statistical and systematic errors

Mean center of mass energy (MeV)	S-factor ($\times 10^{10}$ keV-barns)	Uncertainty ($\times 10^{10}$ keV-barns)
2.933	26.61	1.46
3.185	19.45	0.89
3.437	17.83	0.87
3.689	13.56	0.68
3.941	9.27	0.47
4.193	9.38	0.47
4.445	8.08	0.40
4.696	8.36	0.56
4.797	5.02	0.28
4.948	5.83	0.39
5.200	4.80	0.33
5.451	4.32	0.29
5.954	3.34	0.22
6.456	2.83	0.19
6.958	2.12	0.14
7.961	1.35	0.09
8.463	0.59	0.04

Table 3
Tabulation of the ^{119}Sn(p,γ)^{120}Sb reaction experimental results from this study. Uncertainties include both statistical and systematic errors

Mean center of mass energy (MeV)	S-factor ($\times 10^{10}$ keV-barns)	Uncertainty ($\times 10^{10}$ keV-barns)
2.737	131.7	50.0
2.939	48.4	6.8
3.191	69.8	6.3
3.443	37.8	3.0
3.695	37.0	2.6
3.946	39.2	2.7
4.198	27.6	1.7
4.450	22.8	1.4
4.802	22.0	1.5
5.204	18.8	1.1
5.455	17.1	1.0
5.958	13.0	0.8
6.460	8.75	0.7

with the theoretical prediction although there is some evidence for a higher S-factor at astrophysically significant energies than predicted by NON-SMOKER.

The activation technique used here should be applicable to studying (p,γ) reactions involving other nuclei, including those of higher mass. One difficulty in measuring data on the proton-rich side, however, is the availability of sufficiently isotopically pure targets, since many of the stable nuclei of interest have low abundances. As was seen

Table 4
Tabulation of the $^{96}Zr(p,\gamma)^{97}Nb$ reaction experimental results from this study. Uncertainties include both statistical and systematic errors

Mean center of mass energy (MeV)	S-factor ($\times 10^{10}$ keV-barns)	Uncertainty ($\times 10^{10}$ keV-barns)
3.408	10.76	1.94
3.661	7.93	1.82
3.913	9.20	2.02
4.166	6.34	1.33
4.419	5.16	1.13
4.923	3.62	0.65
5.428	2.49	0.45
5.932	1.46	0.28

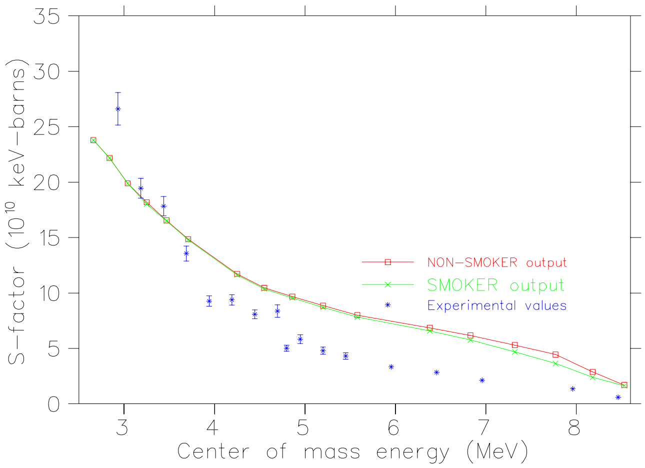

Fig. 7. Deduced and predicted astrophysical S-factors for $^{112}Sn(p,\gamma)^{113}Sb$.

in the case of the ^{119}Sn target, even small impurities can cause difficulty in interpreting the experimental results. Conceivably, this activation technique could be extended to the study of (α,γ) reactions as well, although the high energy needed for the reaction to overcome the Coulomb barrier could result in additional reactions contributing to the decay of the compound nucleus, making the identification of the (α,γ) reaction product more difficult.

Acknowledgements

The authors would like to thank the Indiana University Cyclotron Facility which provided the ^{112}Sn and ^{119}Sn targets used. We would also like to acknowledge the assistance of the Notre Dame University Nuclear Physics Laboratory personnel, especially Larry O. Lamm, for their help and hospitality while making these measurements. The able

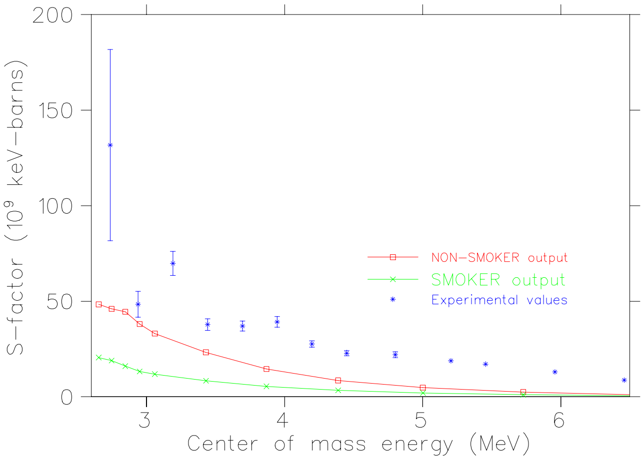

Fig. 8. Deduced and predicted astrophysical S-factors for ^{119}Sn (p,γ)^{120}Sb.

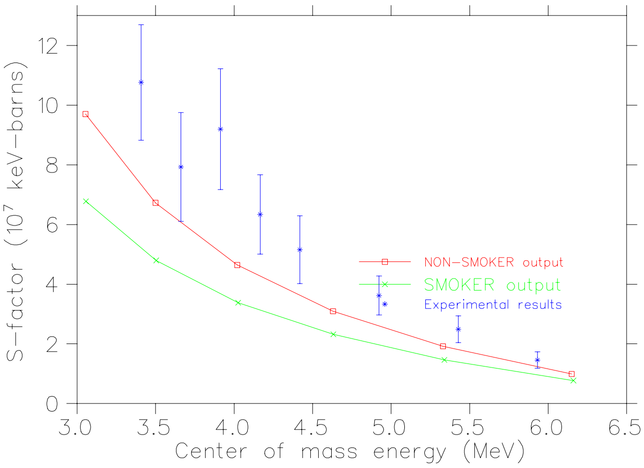

Fig. 9. Deduced and predicted astrophysical S-factors for ^{96}Zr(p,γ)^{97}Nb.

data-taking assistance of M. Famiano is acknowledged for some of the final data checks that were performed. This work was funded by National Science Foundation grants PHY-9513893 and PHY-9402761.

References

[1] S.E. Woosley and W.M. Howard, Astrophys. J. Suppl. 36 (1978) 285.
[2] R.K. Wallace and S.E. Woosley, Astrophys. J. Suppl. 45 (1981) 389.
[3] W.M. Howard, B.S. Meyer and S.E. Woosley, Astrophys. J. 373 (1991) L5.
[4] A.E. Champagne and M. Wiescher, Ann. Rev. Nuc. and Part. Sci. 42 (1992) 39.
[5] S.E. Woosley and R.D. Hoffman, Astrophys. J. 395 (1992) 202.
[6] R.D. Hoffman, S.E. Woosley, G.M. Fuller and B.S. Meyer, Astrophys. J. 460 (1996) 478.
[7] S.E. Woosley, D.H. Hartmann, R.D. Hoffman and W.C. Haxton, Astrophys. J. 356 (1990) 272.

[8] D.L. Lambert, Astron. Astrophys. Rev. 3 (1992) 201.
[9] B.S. Meyer, ARA&A. 32 (1994) 153.
[10] G. Wallerstein, I. Iben, P. Parker, A.M. Boesgaard, G.M. Hale, A.E. Champagne, C.A. Barnes, F. Käppeler, V.V. Smith, R.D. Hoffman, F.X. Timmes, C. Sneden, R.N. Boyd, B.S. Meyer and D.L. Lambert, Rev. Mod. Phys. 69 (1997) 995.
[11] W. Hauser and H. Feshbach, Phys. Rev. 87 (1952) 366.
[12] J. Holmes, S. Woosley, W. Fowler and B. Zimmerman, At. Data and Nuc. Data Tab. 18 (1976) 306.
[13] S. Woosley, W. Fowler, J. Holmes and B. Zimmerman, At. Data and Nuc. Data Tab. 22 (1978) 371.
[14] F.-K. Thielemann, M. Arnould and J.W. Truran, Advances in Nuclear Astrophysics, ed. E. Vangioni-Flam et al. (Editions Frontières, Gif-sur-Yvette, 1986) p. 525.
[15] J. Cowan, F.-K. Thielemann and J. Truran Phys. Rep. 208 (1991) 267.
[16] T. Rauscher, F.-K. Thielemann and K. Kratz, Phys. Rev. C 56 (1997) 1613.
[17] T. Rauscher and F.-K. Thielemann, Stellar Evolution, Stellar Explosions and Galactic Chemical Evolution, ed. T. Mezzacappa (IOP, Bristol, 1998) p. 519.
[18] T. Sauter and F. Käppeler, Phys. Rev. C 55 (1997) 3127.
[19] J. Bork, H. Schatz, F. Käppeler and T. Rauscher, Phys. Rev. C 58 (1998) 524.
[20] C.E. Laird, D. Flynn, R.L. Hershberger and F. Gabbard, Phys. Rev. C 35 (1987) 1265.
[21] E.V. Verdieck and J.M. Miller, Phys. Rev. 152 (1967) 1253.
[22] Zs. Fülöp, A.Z. Kiss, E. Somorjai, C.E. Rolfs, H.P. Trautvetter, T. Rauscher and H. Oberhummer, *in* Nuclei in the Cosmos III, ed. M. Busso, R. Gallino and C. Raiteri (American Institute of Physics Press, New York, 1995).
[23] E. Somorjai, Zs. Fülöp, A.Z. Kiss, C.E. Rolfs, H.P. Trautvetter, U. Greife, M. Junker, S. Goriely, M. Arnould, M. Rayet, T. Rauscher and H. Oberhummer, Astron. Astrophys. 333 (1998) 1112.
[24] T. Rauscher, NON-SMOKER library, http://quasar.physik.unibas.ch/~tommy/reaclib.html.
[25] STOPX and T.C. Awes, Oak Ridge National Laboratory, J.J. Kolata, University of Notre Dame (1983), unpublished.
[26] J.B. Marion and F.C. Young, Nuclear Reaction Analysis: Graphs and Tables (Wiley, New York, 1968).
[27] C.H. Johnson, J.K. Blair, C.M. Jones, S.K. Penny and D.W. Smith, Phys. Rev. C 15 (1977) 196.
[28] N. Ozkan, A.St. J. Murphy, R.N. Boyd, A.L. Cole, M. Famiano, R.T. Guray, M.S. Islam, P. Tischhauser and M.C. Wiescher, private communication.
[29] J.P. Jeukenne, A. Lejeune and C. Mahaux, Phys. Rev. C 15 (1977) 10.